nature nanotechnology

Article

https://doi.org/10.1038/s41565-024-01842-8

Momentum tunnelling between nanoscale liquid flows

Received: 4 June 2024

Accepted: 26 November 2024

Published online: 02 January 2025

Check for updates

Baptiste Coquinot[1,2,7], Anna T. Bui[3,7], Damien Toquer[1], Angelos Michaelides[3], Nikita Kavokine[2,4,5] ✉, Stephen J. Cox[3,6] ✉ & Lydéric Bocquet[1] ✉

The world of nanoscales in fluidics is the frontier where the continuum of fluid mechanics meets the atomic, and even quantum, nature of matter. While water dynamics remains largely classical under extreme confinement, several experiments have recently reported coupling between water transport and the electronic degrees of freedom of the confining materials. This avenue prompts us to reconsider nanoscale hydrodynamic flows under the perspective of interacting excitations, akin to condensed matter frameworks. Here we show, using a combination of many-body theory and molecular simulations, that the flow of a liquid can induce the flow of another liquid behind a separating wall, at odds with the prediction of continuum hydrodynamics. We further show that the range of this 'flow tunnelling' can be tuned through the solid's electronic excitations, with a maximum occurring when these are at resonance with the liquid's charge density fluctuations. Flow tunnelling is expected to play a role in global transport across nanoscale fluidic networks, such as lamellar graphene oxide or MXene membranes. It further suggests exploiting the electronic properties of the confining walls for manipulating liquids via their dielectric spectra, beyond the nature and characteristics of individual molecules.

Nature does many exquisite things with water and ions at small scales. This stunning observation is a source of inspiration and a strong motivation to explore fluidic transport in nanometric confinement. Indeed, over the past 10 years, a cabinet of curiosities of unconventional nanoscale flow properties has been unveiled in nanofluidic studies[1–3]. This prompted many to revisit the standard frameworks of fluid dynamics. While confining walls are merely considered as boundary conditions for hydrodynamics, they are actually 'jiggling and wiggling' matter, being themselves the locus of fluctuations and excitations such as phonons[4–6], plasmons[7,8] and so on. In particular, while the dynamics of liquid water are essentially classical at the molecular scale—grounding our understanding of water transport in classical physics—the confining surfaces may host delocalized electrons, whose behaviour should be described within quantum mechanics. Many experimental studies have now hinted at a non-trivial coupling between the classical water dynamics and the quantum dynamics of these electrons. Prominent examples include flow-induced electronic currents[9–12], the modification of liquid wetting by substrate metallicity[13], heat transfer from graphene electrons to the fluid environment[14], anomalies in hydrodynamic friction at water–carbon interfaces[4,7,8,15–21] and its subtle difference with insulating materials[22].

These findings have shifted perspectives on nanoscale hydrodynamics, prompting a departure from the traditional notion that the solid only acts as a static potential for the liquid molecules, to consider

[1]Laboratoire de Physique de l'Ecole Normale Supérieure, Paris, France. [2]Max Planck Institute for Polymer Research, Mainz, Germany. [3]Yusuf Hamied Department of Chemistry, University of Cambridge, Cambridge, UK. [4]Center for Computational Quantum Physics, Flatiron Institute, New York, NY, USA. [5]The Quantum Plumbing Lab (LNQ), École Polytechnique Fédérale de Lausanne (EPFL), Lausanne, Switzerland. [6]Department of Chemistry, Durham University, Durham, UK. [7]These authors contributed equally: Baptiste Coquinot, Anna T. Bui. ✉e-mail: nikita.kavokine@epfl.ch; stephen.j.cox@durham.ac.uk; lyderic.bocquet@ens.fr

instead the liquid–solid interaction at the level of collective charge density fluctuations. Specifically, polar liquids such as water carry dielectric fluctuations from their collective intermolecular motions, spanning three orders of magnitude in the terahertz (THz) frequency range of the spectrum[23]. For carbon-based materials such as graphene and its multilayers, the THz frequency range is where low-energy electronic surface plasmon modes lie[24,25]. Describing water's interaction with these fluctuations is greatly simplified if its dielectric modes are formally quantized: the corresponding elementary excitations have been dubbed 'hydrons'[10,14]. The excitation perspective for the collective water modes—inspired by many-body condensed matter physics—is at the root of the fluctuation-induced (or 'quantum') friction theory, which has successfully explained several of the phenomena mentioned above[7,8,10,26] and therefore holds the potential to reveal and explain new physics.

Here we show that, as water on one side of a solid wall is driven, the water's excited hydron modes interact with collective modes in the solid substrate. As a result, a flow is induced in the water on the other side of the wall, at odds with the prediction of classical hydrodynamics. We dub this phenomenon 'flow tunnelling'. We develop a complete theoretical and numerical description of flow tunnelling, elucidating the role of the solid's electronic properties in the hydron transmission process and assessing its potential as a new principle for manipulating nanoscale liquid flows.

Flow tunnelling through a passive wall

The system that we consider throughout is shown schematically in Fig. 1a and comprises a liquid water slab on one side of N two-dimensional solid layers ('fluid A'), with another slab of liquid water on the other side ('fluid B'). Before investigating the role of interactions between the solid's and fluid's collective modes in mediating flow tunnelling, we begin with a simpler question: to what extent does a driven flow in fluid A directly induce a flow in fluid B? To this end, we consider the case where the solid layers have no internal degrees of freedom and interact with the fluids only via a static potential. Taking the solid layers to lie in the (x, y) plane, and assuming that fluids A and B flow with in-plane uniform velocities $\mathbf{v}_A$ and $\mathbf{v}_B$, respectively, we ask whether there is a net momentum transfer (or force) from fluid A to fluid B. Such a force would originate from fluctuating Coulomb interactions between water slabs across the passive solid, and its computation in the framework of classical stochastic dynamics would be extremely involved[27,28]. However, it can be readily estimated within an excitation perspective, using a quantum representation of the system.

The thermal charge fluctuations in each slab result in a fluctuating Coulomb potential acting on the other slab that can be decomposed into evanescent plane waves of the form $\phi_{\mathbf{q},\omega}(\mathbf{r}, t) = \phi_0 e^{-qd} e^{i(\mathbf{qr}-\omega t)}$, where $\mathbf{r}$ lies in the (x, y) plane and d is the separation between the outermost solid layers. The elementary bosonic excitations of these modes are the hydrons, in the same way that photons are elementary excitations of the electromagnetic field; $\phi_{\mathbf{q},\omega}$ is then effectively the wavefunction of a hydron. By analogy, since the hydron wavefunctions of fluids A and B overlap, water excitations can 'tunnel' between the two fluids. The hydron transmission rate is then given by the canonical Landauer formula:

$$\Gamma^{A\to B} = \frac{1}{2\pi\hbar}\sum_{\mathbf{q}}\int \mathrm{d}E\,(f^A_{\mathbf{q}}(E) - f^B_{\mathbf{q}}(E))\mathcal{T}_{\mathbf{q}}(E), \tag{1}$$

where $f_{\mathbf{q}}(E)$ is the average number of hydrons of wavevector $\mathbf{q}$ and energy E and $\mathcal{T}_{\mathbf{q}}(E) \propto e^{-2qd}$ is the dimensionless transmission coefficient, which (as a first approximation) scales as the squared overlap of the hydron wavefunctions. If $\mathbf{v}_A = \mathbf{v}_B = 0$, $f^A_{\mathbf{q}}(E) = f^B_{\mathbf{q}}(E) = n_{\mathrm{B}}(\omega = E/\hbar)$, the Bose–Einstein distribution at temperature T, and there is no net hydron transmission from A to B. Now, if $\mathbf{v}_A - \mathbf{v}_B = \Delta\mathbf{v} \neq 0$, the Bose–Einstein distributions experience a Doppler shift $\omega \longmapsto \omega - \mathbf{q}\cdot\mathbf{v}_{A,B}$, so that $\Gamma^{A\to B}$ is non-vanishing. This means that there is indeed a force, or net momentum transfer from A to B, since a hydron of wavevector $\mathbf{q}$ carries a quantum of momentum $\hbar\mathbf{q}$. To linear order in $\Delta\mathbf{v}$, and assuming a single energy scale $\hbar\omega_0 \ll k_{\mathrm{B}}T$ for the hydrons, this force (per unit area) is given by

$$\begin{aligned}\frac{\mathbf{F}_{\mathrm{hh}}}{\mathcal{A}} &\approx \frac{\omega_0}{2\pi}\frac{1}{\mathcal{A}}\sum_{\mathbf{q}}(\hbar\mathbf{q})\,[n_{\mathrm{B}}(\omega_0 - \mathbf{q}\cdot\Delta\mathbf{v}) - n_{\mathrm{B}}(\omega_0)]\,e^{-2qd}\\ &\approx \frac{3k_{\mathrm{B}}T}{16\pi^2\omega_0 d^4}\Delta\mathbf{v}.\end{aligned} \tag{2}$$

F_{hh} is the driving force for the flow tunnelling effect: it induces the flow of fluid B in response to the flow of fluid A. In the steady state, F_{hh} is balanced by the classical (roughness-induced) friction $F_{\mathrm{cl}} = -\lambda_{\mathrm{cl}}\mathcal{A}v_{\mathrm{B}}$ exerted on fluid B by the solid wall, so that

$$v_{\mathrm{B}} = \frac{\lambda_{\mathrm{hh}}}{\lambda_{\mathrm{hh}} + \lambda_{\mathrm{cl}}}v_{\mathrm{A}}, \tag{3}$$

where we have defined the hydron–hydron friction coefficient as $\lambda_{\mathrm{hh}} = F_{\mathrm{hh}}/(\mathcal{A}\Delta v)$. The quantum formalism has enabled us to obtain a first quantitative estimate for flow tunnelling with minimal computations. The final result, however, describes a purely classical effect: Planck's constant is absent from equation (2). We may therefore assess the validity of our description using classical molecular dynamics simulations, where λ_{hh} is directly measured. As shown in Supplementary Information (Supplementary Fig. 4), our prediction in equation (2) matches the simulation results at large separation d between the slabs upon setting $\omega_0 = 0.3$ THz, which is roughly the water Debye frequency. A more accurate analytical result that takes into account the full structure of the water fluctuation spectrum (Supplementary Section IV) agrees with the simulation at arbitrary d.

Although qualitatively at odds with classical hydrodynamics, we find that, quantitatively, this form of flow tunnelling through a passive solid is extremely short-ranged. For example, even assuming small roughness-based friction (for example, $\lambda_{\mathrm{cl}} \approx 2.1 \cdot 10^4$ N s m^{-3} for graphene), we find that v_B is less than 1% of v_A for $d \gtrsim 5$ Å and thus negligible in all practical situations. We now show that the excitations of an 'active' solid (Fig. 1c) drastically enhance the amplitude and range of flow tunnelling, to the extent that it may become experimentally measurable.

The notion that the excitations of a solid wall can mediate momentum transfer between two liquids was in fact suggested more than 50 years ago by Andreev and Meierovich[29]. They considered phononic excitations, whose ability to transfer momentum is limited by the acoustic impedance mismatch between the liquid and the solid: the predicted tunnelling efficiency v_B/v_A is at most ~10^{-5}, whatever the solid thickness (Supplementary Section IV.C). Here we show that the physics are very different in the case of electronic excitations, leading to tunnelling efficiencies up to v_B/v_A ~1.

Molecular simulations of 'active' flow tunnelling

Friction forces that arise from the dynamical coupling between the electronic excitations of the solid and charge density fluctuations in the liquid are nonadiabatic in nature. Such effects are beyond the Born–Oppenheimer approximation typically used in molecular simulations, making the prospect of modelling these with explicit electronic dynamics, on time and length scales relevant to the problem at hand, a daunting task. Recently, however, a classical molecular dynamics scheme was shown to capture the most salient aspects of fluctuation-induced quantum friction[8]. Here we extend this approach to investigate 'active' flow tunnelling, before providing a detailed, yet more general, theoretical account.

The solid wall is modelled as a stack of N layers (with thickness $d = (N-1)d_0$, where d_0 is the spacing between two adjacent layers), with each layer being composed of Lennard-Jones atoms arranged in

https://doi.org/10.1038/s41565-024-01842-8

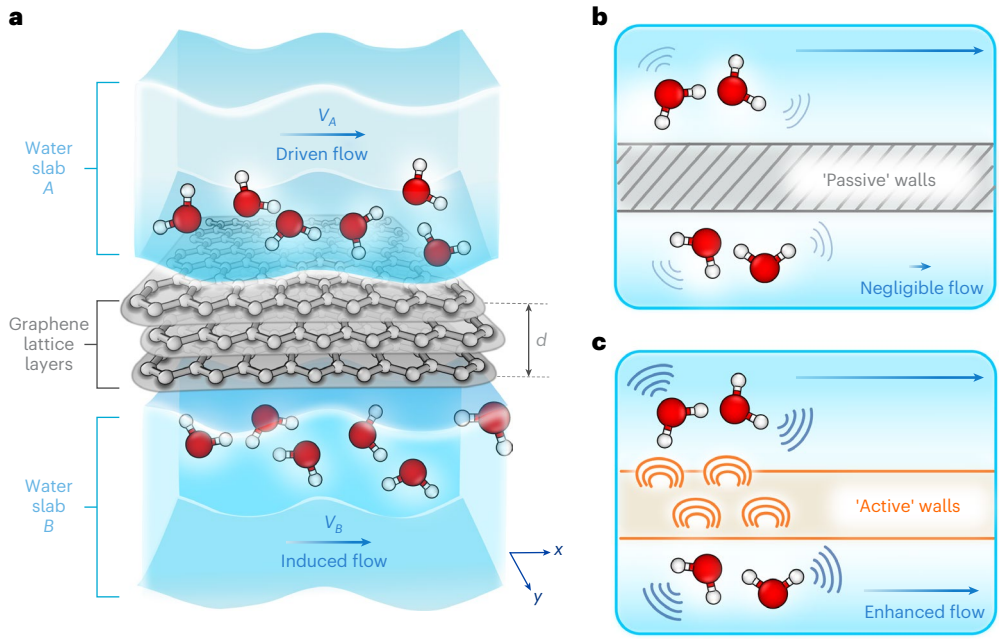

Fig. 1 | Principle of flow tunnelling and role of the solid wall. a, Schematic of the system under study. Two water slabs *A* and *B*, flowing at velocities v_A and v_B, are separated by a solid wall of thickness *d*. **b**, When the wall is 'passive' and only acts as a static potential, water on both sides of the solid can interact via fluctuating Coulomb forces. Direct momentum transfer between two slabs, however, is negligible, so the resulting flow tunnelling effect is very small. **c**, When the wall is 'active' through fluctuations in the solid coming from the electronic degrees of freedom (that is, plasmons), the range and amplitude of flow tunnelling can increase significantly owing to the fluid–solid–fluid coupling.

a honeycomb lattice. Electron dynamics are mimicked by giving each atom a positive charge and attaching to it a fictitious Drude particle of equal and opposite charge via a harmonic spring[30,31] (Fig. 2a). Relaxation processes in the solid (electron–phonon and impurity scattering, umklapp processes[32]) are taken into account implicitly through an effective damping rate γ for the Drude oscillators. This gives the solid prototypical charge fluctuations described by a single plasmon-like mode at a frequency ω_p, which can be adjusted by tuning the mass of the Drude particle. While the Drude model is a crude representation for a realistic plasmon and its dispersion behaviour, it allows us to capture the essential physics since its principal mode can be tuned to overlap in frequency with the water's surface response (Fig. 2b), thereby controlling the degree of dynamical coupling between the solid and the liquid. As seen in Fig. 2c, as ω_p approaches the THz regime from above, the total solid–liquid friction increases from its 'classical' surface-roughness value λ_{cl}: this extra contribution is the fluctuation-induced (quantum) friction λ_{qf} (refs. 7,8). Momentum transfer from the liquid to the solid is therefore enhanced by matching the frequencies of their respective charge fluctuations.

We then performed non-equilibrium molecular dynamics simulations with a pressure gradient applied to fluid *A* and measured the resulting non-equilibrium steady-state flow velocities in both fluids *A* and *B*. In the absence of Drude oscillators, no induced flow in fluid *B* could be measured for a solid thicker than a single layer, in line with our prediction in equations (2) and (3). However, when the Drude frequency was set in the range of water's Debye modes, we observed a large induced flow even through much thicker solids, up to $N = 7$ layers (Fig. 2d). For example, $v_B \approx 0.1\, v_A$ for a 2-nm-thick ($N = 7$) solid with $\omega_p = 0.1$ THz and relaxation rate $\gamma = 10^{-3}$ THz. The induced velocity v_B scaled linearly with the driven velocity v_A in the investigated range (Fig. 2d).

Our simulations thus reveal that the coupling to the solid's charge fluctuation modes does not simply take momentum away from fluid *A* through friction. Momentum is in fact accumulated in those modes, and part of it is transmitted to fluid *B*, resulting in flow tunnelling. The amount of momentum accumulation is sensitive to the relaxation rate γ, with faster relaxation leading to weaker flow tunnelling (Fig. 2e). While in our simulations, the Drude particles themselves do not flow, in a real solid, there would be propagation of both collective plasmons and single electrons. The latter would induce an electric current parallel to the surface, akin to the Coulomb drag phenomenon[33]. We finally note that the momentum transfer is measured to be important despite the fluid flow being transverse to the direction of momentum transfer across the layers, a point further confirmed by the theoretical modelling.

Many-body quantum theory of flow tunnelling

Guided by the simulation results, we now develop a theory of flow tunnelling through an active solid. Within our formally quantum picture, flow tunnelling through a passive solid amounted to coherent hydron transport between the two fluids—it was therefore described by a Landauer formula. The active solid now plays the role of a 'junction' placed between the two hydron reservoirs (the fluids). As highlighted by the strong dependence of the simulation results on the relaxation parameter γ, the hydron transport through this junction cannot be considered coherent, and its description therefore requires going beyond the Landauer formalism. To account for decoherence, we model the solid by a layered structure in our simulations. The hydrons are transported coherently between the layers, but they can undergo inelastic scattering (that is, decoherence) within each of the layers. Technically, we use the Keldysh formalism of perturbation theory, which has proven to be an asset in the study of non-equilibrium solid–liquid systems[7,10]. Our computation is fully detailed in Supplementary Sections III–V; here we outline the main steps.

The system is described in terms of the fluctuating charge densities $n(\mathbf{r}, t)$ of both the liquid slabs and the solid layers. It is governed by the Hamiltonian comprising all Coulomb interactions: between the water and the solid, between the two water slabs and between the different solid layers. To keep the computations tractable, we assume that a solid layer interacts only with its nearest neighbours (Fig. 3a).

https://doi.org/10.1038/s41565-024-01842-8

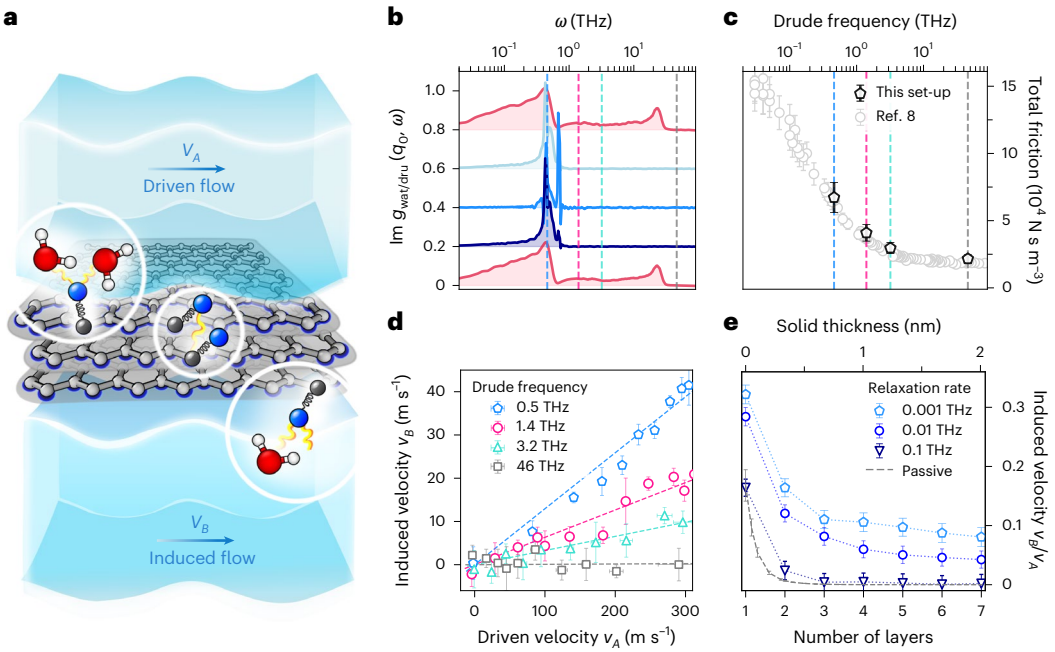

Fig. 2 | Molecular simulations of flow tunnelling. a, Schematic representation of the system simulated with Drude oscillators, used as a classical proxy for the quantum electron dynamics. **b**, The surface excitation spectra as measured in simulations of each component in an $N = 3$ system: water slab A, each solid layer and water slab B going from top to bottom. Here the wavevector is $q_0 = 2.5$ nm^{-1} and the Drude frequency is $\omega_p = 0.5$ THz. The vertical lines indicate the other tested frequencies for the Drude oscillators. **c**, The total solid–liquid friction corresponding to the different Drude frequencies ω_p chosen for a system with $N = 3$, compared with the result for a single water slab on a single graphene sheet in ref. 8. The similarity of the results indicates that the friction is essentially determined by the interaction with the first solid layer. **d**, Induced velocity through $N = 3$ layers of solid v_B versus imposed velocity v_A for the different Drude frequencies ω_p, and fixed relaxation rate $\gamma = 10^{-3}$ THz. **e**, Tunnelling efficiency v_B/v_A as a function of the number of layers N for different relaxation rates γ and fixed Drude frequency $\omega_p = 0.5$ THz (in blue) and through a passive solid (in grey). From our simulations, the standard error was obtained from splitting the trajectory into at least three blocks.

Our goal is to evaluate the average Coulomb force exerted by the Nth solid layer on the fluid slab B, in the non-equilibrium state where fluid A flows at velocity v_A:

$$\mathbf{F}_{NB} = \int \mathrm{d}\mathbf{r}_N \mathrm{d}\mathbf{r}_B \langle n_N(\mathbf{r}_N, t) V(\mathbf{r}_N - \mathbf{r}_B) n(\mathbf{r}_B, t) \rangle, \tag{4}$$

where $\mathbf{r}_N$ and $\mathbf{r}_B$ are the spatial coordinates in layer N and fluid slab B, respectively, and V is the Coulomb potential. To this end, we formally quantize the charge densities as free Gaussian fields—this is an approximation that amounts to neglecting interactions between excitations. The liquid and the solid are then fully characterized by their charge density correlation functions, which can be evaluated starting from the microscopic model of one's choice. In the following, we will describe the solid by the correlation function of the Drude oscillator model, to allow for direct comparison with the simulations. However, one could model each solid layer as a two-dimensional electron gas with appropriate electron–electron and electron–phonon interactions (accounting for decoherence), so as to describe realistic solid-state systems that cannot be treated classically, such as few-layer transition metal dichalcogenides or MXenes.

The model defined in this way is in fact integrable (the Hamiltonian is quadratic in the charge densities), so that the non-equilibrium state of the system can be determined exactly using the Keldysh formalism. In practice, we perturbatively expand the average in equation (4) in powers of the Coulomb interaction and exactly resum the infinitely many terms of this expansion. The basic building blocks of the expansion are the surface response functions g of each of the water slabs and solid layers. These are appropriately normalized charge density correlation functions: $g(\mathbf{q}, \omega) \sim V_q \langle n_{\mathbf{q}} n_{-\mathbf{q}} \rangle_\omega$, where $V_q = e^2/(2\epsilon_0 q)$ is the Fourier-transformed Coulomb potential and $n_{\mathbf{q}}$ are charge density operators. Precise definitions of these quantities are given in Supplementary Section III.C. In the Keldysh formalism, these correlation functions possess three components (g^R, g^A and g^K), corresponding to different time orderings of the operators. In the non-interacting equilibrium state, the Drude response function of a solid layer is

$$g^R_{\mathrm{eq,\,Drude}} = \frac{\omega_p^2 f(q)}{\omega_p^2 - \omega^2 - 2i\gamma\omega}, \tag{5}$$

and the water surface response function is modelled, following ref. 7, as a sum of two Debye peaks:

$$g^R_{\mathrm{eq,\,Water}} = \sum_{i=1,2} \frac{f_i(q)}{1 - i\omega/\omega_{\mathrm{D},i}}. \tag{6}$$

The values of the parameters and expressions of the functions $f(q)$ are given in Supplementary Section IV. The imposed flow in the fluid A and the induced flow in the fluid B are described, as before, by a Doppler shift in the non-equilibrium water surface response function versus its equilibrium expression: $g(\mathbf{q}, \omega) = g_{\mathrm{eq}}(\mathbf{q}, \omega - \mathbf{q} \cdot \mathbf{v}_{A,B})$. The expansion proceeds in two steps. First, the non-equilibrium response functions of the N solid layers are determined by solving a series of Dyson equations, accounting for the inter-layer coupling via the electrostatic interactions and decoherence process throughout the solid. These equations have a very simple diagrammatic representation (Fig. 3b)—since the Hamiltonian is quadratic in the density operators—and they are algebraic in Fourier space. For example, the renormalization of the layer $i+1$ by the layer i for the retarded component is given by $g^R_{i+1} = g^{R,\mathrm{eq}}_{i+1} + g^{R,\mathrm{eq}}_{i+1} g^R_i g^R_{i+1}$, and the expression for the Keldysh component is given in Supplementary Section III.D. Then, the expansion of

https://doi.org/10.1038/s41565-024-01842-8

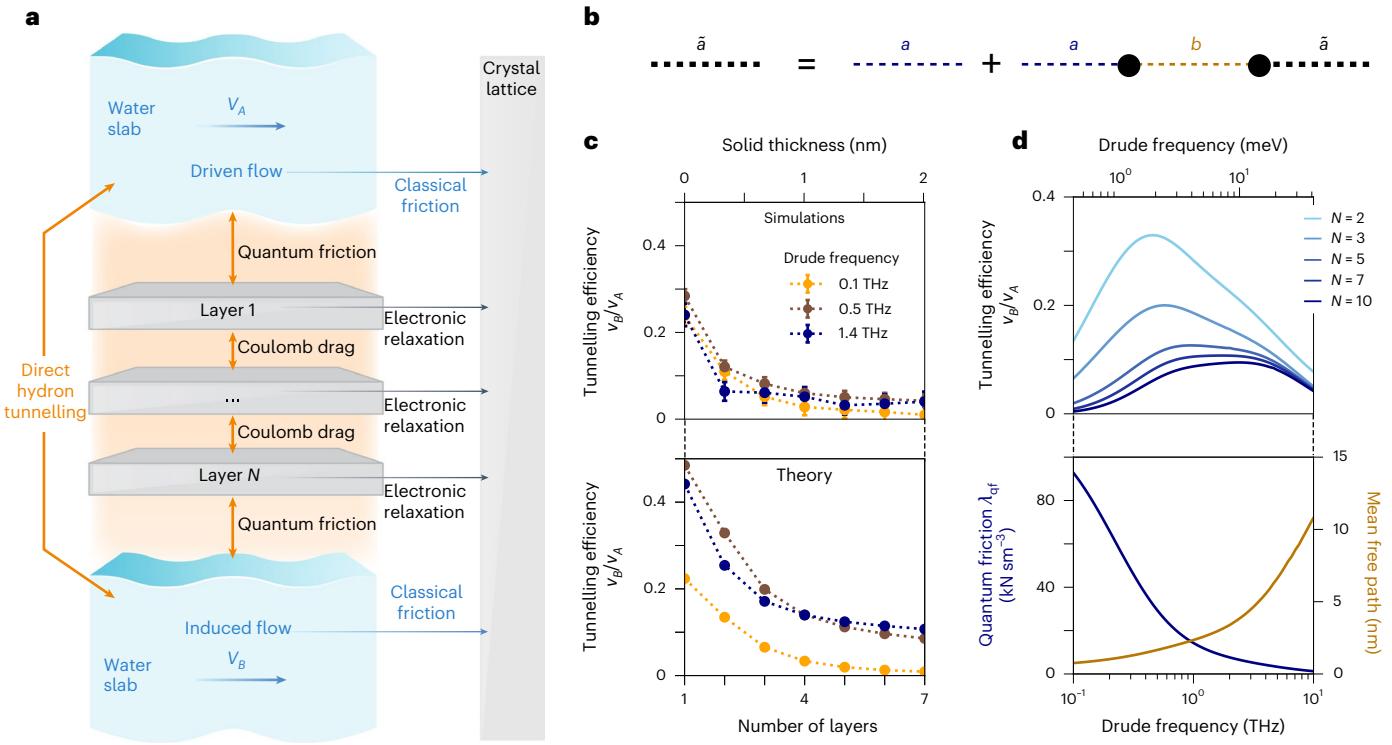

Fig. 3 | Quantum theory of flow tunnelling. a, Diagram representing the momentum fluxes in the liquid–solid–liquid system. Momentum can be transferred from fluid *A* to fluid *B* sequentially through the *N* solid layers, or through direct hydron tunnelling if the solid is thin. The processes that dissipate momentum are represented by the horizontal arrows. **b**, Dyson equation for the surface response function of layer *a* renormalized by the interactions with layer *b*. A thin line represents a bare response function (in blue for *a* and gold for *b*), while the black thick lines represent the renormalized response function of *a*. **c**, Tunnelling efficiency v_B/v_A as a function of the number of layers for different Drude frequencies ω_p and a relaxation rate of $\gamma = 10^{-2}$ THz. Top: simulation data. From our simulations, the standard error was obtained from splitting the trajectory into at least three blocks. Bottom: theoretical prediction. **d**, Tunnelling efficiency v_B/v_A (top) as a function of the Drude frequency ω_p for a relaxation rate of $\gamma = 10^{-2}$ THz. There is an optimal Drude frequency because of the trade-off between the two quantities plotted at the bottom: the quantum friction coefficient (in blue) and the hydron mean free path inside the solid (in gold).

equation (4) is carried out in terms of those response functions, yielding the force acting on the *B* fluid across the *N* layers of material:

$$\frac{\mathbf{F}_{NB}}{\mathcal{A}} = \int \frac{\mathrm{d}\mathbf{q}}{(2\pi)^2}(\hbar\mathbf{q})(\Gamma_{NB}(\mathbf{q}) - \Gamma_{BN}(\mathbf{q})) \tag{7}$$

with

$$\Gamma_{\mathrm{ab}}(\mathbf{q}) = \int \frac{\mathrm{d}\omega}{4i\pi} \frac{\mathrm{Im}[g_{\mathrm{a}}^{\mathrm{R}}(\mathbf{q},\omega)]g_{\mathrm{b}}^{\mathrm{K}}(\mathbf{q},\omega)}{|1 - g_{\mathrm{a}}^{\mathrm{R}}(\mathbf{q},\omega)g_{\mathrm{b}}^{\mathrm{R}}(\mathbf{q},\omega)|^2}. \tag{8}$$

Equations (7) and (8) are our main theoretical result, which has general validity beyond the particular Drude model of the solid that we have considered so far. It is a far-from-equilibrium generalization of quantum friction[7], which echoes the Landauer formula in equation (1). For true interacting electrons, our result is valid at the level of a self-consistent Hartree approximation. $\mathbf{F}_{NB}$ depends on both v_A and v_B and can be expanded to linear order in these velocities, defining two friction coefficients: $\mathbf{F}_{NB}/\mathcal{A} = \lambda_{\mathrm{drive}}\mathbf{v}_A - \lambda_{\mathrm{qf}}\mathbf{v}_B$. The coefficient λ_{qf} is the fluctuation-induced (quantum) friction coefficient between the fluid slab *B* and the *N*th solid layer at equilibrium. The coefficient λ_{drive} accounts for the 'remote drag' exerted by fluid *A* on fluid *B*—its expression is cumbersome (Supplementary Section V), but we provide in the following a scaling estimate that allows us to draw practical conclusions.

Physically, the solid gives momentum to the liquid but then takes some of it back through quantum friction. Fluid *B* is also subject to an additional force owing to direct hydron tunnelling (λ_{hh}) if the solid is thin, and to the classical roughness-based friction (λ_{cl}) on the *N*th layer. Momentum conservation then imposes

$$\mathbf{v}_B = \frac{\lambda_{\mathrm{drive}} + \lambda_{\mathrm{hh}}}{\lambda_{\mathrm{qf}} + \lambda_{\mathrm{cl}} + \lambda_{\mathrm{hh}}}\mathbf{v}_A. \tag{9}$$

Equation (9) is our theoretical prediction for the flow tunnelling effect. In Fig. 3c, we compare the theoretical predictions against simulation results. Given the simplifying assumptions in the theoretical model (that is, nearest-neighbour interactions between graphene layers, and a harmonic approximation for water's dielectric fluctuations), the agreement is remarkable and suggests that equation (9) captures the essential physics of the flow tunnelling effect.

Conditions for optimal flow tunnelling

Having established a theoretical framework, we may now assess the precise role of the solid's electronic properties in determining the range of flow tunnelling. Figure 3d shows the prediction for the tunnelling efficiency v_B/v_A as a function of the Drude plasmon frequency ω_p, at fixed $\gamma = 10^{-2}$ THz. Interestingly, it exhibits a maximum at $\omega_p \sim 0.3$ THz where the Drude frequency is in resonance with the water Debye frequency (Fig. 2b). Moreover, we observe that at small ω_p, the flow tunnelling efficiency decreases with an increasing number of solid layers *N*, while at large ω_p, it is nearly independent of *N* for $N \leq 7$.

These features can be understood if flow tunnelling is represented as the transmission of discrete excitations—hydrons—between fluid *A* and fluid *B*. In equation (9), the friction coefficient λ_{drive} is effectively the rate at which the solid injects momentum-carrying hydrons into fluid *B*. Hydrons are injected into the solid from fluid *A* with a rate λ_{qf}. However, they only reach fluid *B* if they are not scattered during their residence time τ inside the solid, which happens at a rate γ. If the solid is moderately thin, hydrons reach the opposite boundary quickly, and

τ is the time it takes for a hydron to exit into fluid B: $\tau \approx \tau_{sl} \sim \lambda_{qf}^{-1}$. For thicker solids, most hydrons get scattered on their way from A to B so that $\tau \propto N$, and we may define a mean free path ℓ according to $\gamma\tau \equiv d/\ell$. Altogether (and assuming $N > 1$ so that λ_{hh} can be neglected), we obtain an asymptotic expression for the tunnelling efficiency, valid for thick solids:

$$\frac{v_B}{v_A} \approx \frac{\lambda_{qf}}{\lambda_{qf} + \lambda_{cl}} e^{-(\gamma\tau_{sl} + d/\ell)}, \tag{10}$$

with τ_{sl} and ℓ both depending on the Drude frequency ω_p and relaxation rate γ. For thin solids (small N, as in our simulations), we obtain a more accurate scaling expression that accounts for the discreteness of the layers (Supplementary Section V.D), but the data is still well described by equation (10) (Supplementary Fig. 6f). Within the Drude model of the solid, λ_{qf} is a strictly decreasing function of ω_p (Fig. 3d): hydron injection into the solid is most efficient for lower Drude frequencies. However, the hydron mean free path is shorter for lower ω_p (Fig. 3d): lower frequency modes take longer to transmit their excitations to the next layer. The thicker the solid, the more flow tunnelling is favoured by higher plasmon frequencies. This trade-off between hydron injection rate and mean free path accounts for the 'resonant', bell-shaped dependence of the tunnelling efficiency on ω_p.

Going further, the result in equation (10) allows us to draw general conclusions regarding the range of flow tunnelling. This range is limited by the scattering rate γ of excitations inside the solid: flow can in principle tunnel through an arbitrarily thick solid if there is no dissipation inside. This is never the case in practice, and no tunnelling is observed if the solid is thicker than a few times the mean free path ℓ. For $d \gtrsim \ell$, the tunnelling efficiency decreases exponentially with d (Fig. 3c at low ω_p): the hydron transport is diffusive. However, the mean free path can sometimes become very large (Fig. 3d at large ω_p). Then, it is realistic to have $d \ll \ell$, and the hydron transport becomes ballistic. The tunnelling efficiency is then limited by the solid–liquid crossing time $\tau_{sl} \sim \lambda_{qf}^{-1}$: hydrons are scattered as they wait in the solid to cross into fluid B. v_B/v_A is then independent of d as seen in Fig. 3d at high Drude frequencies. But in both the diffusive and the ballistic regimes, the tunnelling efficiency is ultimately determined by comparing the residence time of an excitation inside the solid to its inelastic scattering (or dephasing) rate.

We have thus identified the three qualitative determinants of flow tunnelling: hydron injection rate, hydron mean free path ℓ and hydron exit rate τ_{sl}^{-1}, which combine to predict the tunnelling efficiency in equation (10). We may now discuss the possibility of flow tunnelling in a realistic solid–liquid system—such as two slabs of water separated by a graphene multilayer—based on these three ingredients. Within our model, the hydron injection rate is set by the quantum friction coefficient λ_{qf}. However, this ignores electron–phonon coupling in the solid and the resulting phonon drag effect[10], which effectively replaces λ_{qf} by ~λ_{cl} in equation (10). Because the electron–phonon and electron–hydron scattering rates typically have similar values[10], we further expect $\gamma\tau_{sl}$ ~1. Therefore, the one key determinant of the tunnelling efficiency is in fact the hydron mean free path, for which our theory may provide a quantitative estimate (Supplementary Section V.D): in the Drude model framework, we find the phenomenological scaling $\ell \approx \ell_0\sqrt{\omega_p/\gamma}$, with $\ell_0 = 0.26$ nm. Ignoring dispersion effects, the graphene plasmon mode may be approximately described by $\omega_p = 100$ THz and $\gamma = 0.6$ THz (ref. 34), yielding $\ell \approx 4$ nm. We note that this is likely an underestimation, as it ignores electron transport perpendicular to the graphene layers. Overall, we may expect non-negligible flow tunnelling through a 10-nm-thick graphene wall, which can be readily obtained in nanofluidic systems using, for example, van der Waals assembly.

Conclusion

Using a combination of many-body quantum theory and molecular simulations, we have shown that the flow of one liquid can induce the flow of another liquid through a solid wall of nanoscale thickness—a phenomenon termed 'flow tunnelling'. Classical hydrodynamics have so far been found to hold surprisingly well down to 1 nm wide channels. Our prediction implies that, in systems of multiple channels, the classical framework of hydrodynamics may qualitatively break down if the walls separating the channels are thinner than ~10 nm. The physical origin of this breakdown lies in the coupling of the liquid charge fluctuations to the solid wall's electronic excitations. Beyond the fundamental importance of flow tunnelling as an effect beyond hydrodynamics, this property is expected to be at play in global transport across nanoscale fluidic networks, in particular across membranes made of lamellar materials such as graphene oxides or MXenes[35,36]. Flow tunnelling is also a new and promising lever for manipulating liquids at the nanoscale via their dielectric spectrum, and not based on the nature and characteristics of individual molecules.

Online content

Any methods, additional references, Nature Portfolio reporting summaries, source data, extended data, supplementary information, acknowledgements, peer review information; details of author contributions and competing interests; and statements of data and code availability are available at https://doi.org/10.1038/s41565-024-01842-8.

References

1. Aluru, N. R. et al. Fluids and electrolytes under confinement in single-digit nanopores. *Chem. Rev.* **123**, 2737–2831 (2023).
2. Faucher, S. et al. Critical knowledge gaps in mass transport through single-digit nanopores: a review and perspective. *J. Phys. Chem. C* **123**, 21309–21326 (2019).
3. Bocquet, L. Nanofluidics coming of age. *Nat. Mater.* **19**, 254–256 (2020).
4. Ma, M. et al. Water transport inside carbon nanotubes mediated by phonon-induced oscillating friction. *Nat. Nanotechnol.* **10**, 692–695 (2015).
5. Marbach, S., Dean, D. S. & Bocquet, L. Transport and dispersion across wiggling nanopores. *Nat. Phys.* **14**, 1108–1113 (2018).
6. Lizée, M., Coquinot, B., Mariette, G., Siria, A. & Bocquet, L. Anomalous friction of supercooled glycerol on mica. *Nat. Commun.* **15**, 6129 (2024).
7. Kavokine, N., Bocquet, M.-L. & Bocquet, L. Fluctuation-induced quantum friction in nanoscale water flows. *Nature* **602**, 84–90 (2022).
8. Bui, A. T., Thiemann, F. L., Michaelides, A. & Cox, S. J. Classical quantum friction at water–carbon interfaces. *Nano Lett.* **23**, 580–587 (2023).
9. Lizée, M. et al. Strong electronic winds blowing under liquid flows on carbon surfaces. *Phys. Rev. X* **13**, 011020 (2023).
10. Coquinot, B., Bocquet, L. & Kavokine, N. Quantum feedback at the solid–liquid interface: flow-induced electronic current and its negative contribution to friction. *Phys. Rev. X* **13**, 011019 (2023).
11. Rabinowitz, J., Cohen, C. & Shepard, K. L. An electrically actuated, carbon-nanotube-based biomimetic ion pump. *Nano Lett.* **20**, 1148–1153 (2020).
12. Yin, J. et al. Generating electricity by moving a droplet of ionic liquid along graphene. *Nat. Nanotechnol.* **9**, 378–383 (2014).
13. Comtet, J. et al. Nanoscale capillary freezing of ionic liquids confined between metallic interfaces and the role of electronic screening. *Nat. Mater.* **16**, 634–639 (2017).
14. Yu, X., Principi, A., Tielrooij, K.-J., Bonn, M. & Kavokine, N. Electron cooling in graphene enhanced by plasmon–hydron resonance. *Nat. Nanotechnol.* **18**, 898–904 (2023).
15. Majumder, M., Chopra, N., Andrews, R. & Hinds, B. J. Enhanced flow in carbon nanotubes. *Nature* **438**, 44–44 (2005).
16. Holt, J. K. et al. Fast mass transport through sub-2-nanometer carbon nanotubes. *Science* **312**, 1034–1037 (2006).

17. Maali, A., Cohen-Bouhacina, T. & Kellay, H. Measurement of the slip length of water flow on graphite surface. *Appl. Phys. Lett.* **92**, 053101 (2008).
18. Secchi, E. et al. Massive radius-dependent flow slippage in carbon nanotubes. *Nature* **537**, 210–213 (2016).
19. Xie, Q. et al. Fast water transport in graphene nanofluidic channels. *Nat. Nanotechnol.* **13**, 238–245 (2018).
20. Keerthi, A. et al. Water friction in nanofluidic channels made from two-dimensional crystals. *Nat. Commun.* **12**, 3092 (2021).
21. Coquinot, B., Becker, M., Netz, R. R., Bocquet, L. & Kavokine, N. Collective modes and quantum effects in two-dimensional nanofluidic channels. *Faraday Discuss.* **249**, 162–180 (2023).
22. Tocci, G., Joly, L. & Michaelides, A. Friction of water on graphene and hexagonal boron nitride from ab initio methods: very different slippage despite very similar interface structures. *Nano Lett.* **14**, 6872–6877 (2014).
23. Heyden, M. et al. Dissecting the THz spectrum of liquid water from first principles via correlations in time and space. *Proc. Natl Acad. Sci. USA* **107**, 12068–12073 (2010).
24. Hafez, H. A. et al. Extremely efficient terahertz high-harmonic generation in graphene by hot Dirac fermions. *Nature* **561**, 507–511 (2018).
25. Ju, L. et al. Graphene plasmonics for tunable terahertz metamaterials. *Nat. Nanotechnol.* **6**, 630–634 (2011).
26. Coquinot, B., Bocquet, L. & Kavokine, N. Hydroelectric energy conversion of waste flows through hydroelectronic drag. *Proc. Natl Acad. Sci. USA* **121**, e2411613121 (2024).
27. Dean, D. S. & Gopinathan, A. Out-of-equilibrium behavior of Casimir-type fluctuation-induced forces for free classical fields. *Phys. Rev. E* **81**, 041126 (2010).
28. Chen, W., Andreev, A. V. & Levchenko, A. Boltzmann–Langevin theory of Coulomb drag. *Phys. Rev. B* **91**, 245405 (2015).
29. Andreev, A. F. & Meierovich, A. E. Dragging of a liquid by a liquid through a stationary solid wall. *JETP Lett.* **15**, 39 (1971).
30. Lamoureux, G. & Roux, B. Modeling induced polarization with classical Drude oscillators: theory and molecular dynamics simulation algorithm. *J. Chem. Phys.* **119**, 3025–3039 (2003).
31. Misra, R. P. & Blankschtein, D. Insights on the role of many-body polarization effects in the wetting of graphitic surfaces by water. *J. Phys. Chem. C* **121**, 28166–28179 (2017).
32. Kittel, C. *Introduction to Solid State Physics* (Wiley, 2004).
33. Narozhny, B. N. & Levchenko, A. Coulomb drag. *Rev. Mod. Phys.* **88**, 025003 (2016).
34. Ni, G. X. et al. Fundamental limits to graphene plasmonics. *Nature* **557**, 530–533 (2018).
35. Ouyang, W., Hod, O. & Urbakh, M. Parity-dependent moiré superlattices in graphene/h-BN heterostructures: a route to mechanomutable metamaterials. *Phys. Rev. Lett.* **126**, 216101 (2021).
36. Gogotsi, Y. & Anasori, B. The rise of MXenes. *ACS Nano* **13**, 8491–8494 (2019).

Data availability

The simulation data that support the findings of this study are openly available at the University of Cambridge Data Repository at https://doi.org/10.17863/CAM.113204.

Acknowledgements

We thank M. Bonn for many fruitful discussions. We thank L. Reading-Ikkanda for help with figure preparation. We are also grateful for computational support from the UK national high performance computing service, ARCHER2, for which access was obtained via the UKCP consortium and funded by EPSRC grant reference EP/X035891/1. B.C., D.T., A.M. and L.B. acknowledge support from ERC project n-AQUA, grant agreement 101071937. B.C. acknowledges support from the CFM Foundation. A.T.B. acknowledges funding from the Oppenheimer Fund and Peterhouse College, University of Cambridge. The Flatiron Institute is a division of the Simons Foundation. S.J.C. is a Royal Society University Research Fellow (grant number URF\R1\211144).

Author contributions

A.M., N.K., S.J.C. and L.B. conceptualized the project. B.C. carried out the theoretical analysis. A.T.B. designed and performed the molecular simulations. D.T. performed the supporting analyses. B.C., A.T.B., A.M., N.K., S.J.C. and L.B. wrote the paper.

Competing interests

The authors declare no competing interests.

Additional information

Supplementary information The online version contains supplementary material available at https://doi.org/10.1038/s41565-024-01842-8.

Correspondence and requests for materials should be addressed to Nikita Kavokine, Stephen J. Cox or Lydéric Bocquet.

Peer review information *Nature Nanotechnology* thanks Zhiping Xu and the other, anonymous, reviewer(s) for their contribution to the peer review of this work.